

# Thermal Hall effect driven by phonon-magnon hybridization in a honeycomb antiferromagnet

Qingkai Meng<sup>1</sup>, Xiaokang Li<sup>1,\*</sup>, Lingxiao Zhao<sup>2</sup>, Chao Dong<sup>1</sup>, Zengwei Zhu<sup>1,\*</sup> and Kamran Behnia<sup>3,\*</sup>

(1) Wuhan National High Magnetic Field Center, School of Physics,  
Huazhong University of Science and Technology, 430074 Wuhan, China

(2) Quantum Science Center of Guangdong-HongKong-Macao Greater Bay Area, 518045 Shenzhen, China

(3) Laboratoire de Physique et d'Étude des Matériaux  
(ESPCI - CNRS - Sorbonne Université), PSL Research University, 75005 Paris, France

(Dated: March 21, 2024)

The underlying mechanism of the thermal Hall effect (THE) generated by phonons in a variety of insulators is yet to be identified. Here, we report on a sizeable thermal Hall conductivity in NiPS<sub>3</sub>, a van de Waals stack of honeycomb layers with a zigzag antiferromagnetic order below  $T_N = 155$  K. The longitudinal ( $\kappa_{aa}$ ) and the transverse ( $\kappa_{ab}$ ) thermal conductivities peak at the same temperature and the thermal Hall angle ( $\kappa_{ab}/\kappa_{aa}/B$ ) respects a previously identified bound. The amplitude of  $\kappa_{ab}$  is extremely sensitive to the amplitude of magnetization along the  $b$ -axis, in contrast to the phonon mean free path, which is not at all. We show that the magnon and acoustic phonon bands cross each other along the  $b^*$  orientation in the momentum space. The exponential temperature dependence of  $\kappa_{ab}$  above its peak reveals an energy scale on the order of magnitude of the gap expected to be opened by magnon-phonon hybridization. This points to an intrinsic scenario for THE with possible relevance to other magnetic insulators.

The thermal analog of electrical Hall effect is dubbed thermal Hall effect (THE). It refers to a transverse temperature difference generated by a longitudinal heat current in presence of a perpendicular magnetic field. For a long time, phonons, lacking charge and spin, were thought incapable of contributing to the THE [1]. However, this assumption was proven wrong by the discovery of a THE in a paramagnetic insulator (Tb<sub>3</sub>Ga<sub>3</sub>O<sub>12</sub>) in 2005 [2]. Numerous experiments [3–20] have reported on a detectable THE in a wide variety of insulators, including three non-magnetic solids [10, 18, 20]. These experimental observations motivated many theoretical studies on how the lattice vibrations (phonons) can couple to the magnetic field [1, 21–31]. The main proposals can be broadly classified as extrinsic, invoking scattering of phonons, or intrinsic, referring to dispersion of phonons.

NiPS<sub>3</sub> is a layered antiferromagnet, with Ni atoms forming a honeycomb lattice (See Fig. 1 a) stacked on top of each other and coupled by van der Waals interaction [32, 33]. Its zigzag antiferromagnetic order can be described by a Hamiltonian with ferromagnetic exchange between the first and the third neighbors and a much weaker antiferromagnetic exchange between the second neighbors [34, 35]. It has an energy gap of 1.8 eV [33] and belongs to the the family of  $MPX_3$  ( $M = \text{Fe, Mn, Ni, and } X = \text{S, Se}$ ) van der Waals magnets. The discovery of spin-orbit-entangled excitons associated with a Zhang-Rice singlet-triplet transition [36], has amplified the interest in this family as a platform for studying many-body coherence and coupling [37–40]. Recently, infrared and Raman spectroscopy detected hybridization between magnon and optical phonon bands in FePSe<sub>3</sub> [37, 39, 40].

Here, we present a study of thermal transport in NiPS<sub>3</sub> crystals. The thermal Hall conductivity,  $\kappa_{ab}$ , peaks to a value large as -1.64 W/Km at 25 K and 14 T, close to

the largest ever recorded [18]. The longitudinal ( $\kappa_{aa}$ ) and transverse ( $\kappa_{ab}$ ) thermal conductivities peak at the same temperature. The thermal Hall angle ( $\frac{1}{B} \frac{\kappa_{ab}}{\kappa_{aa}}$ ) remains within a narrow range of  $10^{-4}$ - $10^{-3} T^{-1}$ . These features are shared by other insulators reported to display a THE [10, 14, 18], including non-magnetic ones. A novel and revealing observation is the striking contrast between the sensitivity of the transverse (and the insensitivity of the longitudinal) thermal conductivity to the in-plane anisotropy of magnetic susceptibility. A thirty percent variation in the amplitude of magnetization along  $b$ -axis leaves the in-plane longitudinal thermal conductivity (which is isotropic) unchanged, but leads to an almost ten-fold increase in  $\kappa_{ab}$ . This means that the amplitude of  $\kappa_{ab}$  correlates with a thermodynamic property, i.e the field-derivative of the free energy, providing strong evidence for an intrinsic origin. This hypothesis is backed by comparing the computed phonon dispersion with the experimentally extracted magnon spectrum. we show that along  $b^*$  in the reciprocal space, an acoustic phonon band and a magnon band in NiPS<sub>3</sub> cross at an energy of 3.7 meV. Interestingly, the temperature dependent of THE above its peak points to a gap of 26 K, strengthening further the case of magnon-phonon hybridization as the source of chirality.

NiPS<sub>3</sub> single crystals used in this work were grown by the chemical vapor transport method using I<sub>2</sub> as the transport agent (see the supplement for more details [41]). The temperature dependence of the magnetization can be seen in Figure 1b. The Néel temperature is 155 K and the easy axis along  $a$ . These features are consistent with the previous report [32, 35, 36]. As seen in Figure 1c, The field dependence of magnetization up to 55 T (at 4.2 K) does not show any transition. This implies the Zeeman energy at this field (estimated to be 3.2 meV), does not destroy the magnetic order. Therefore,

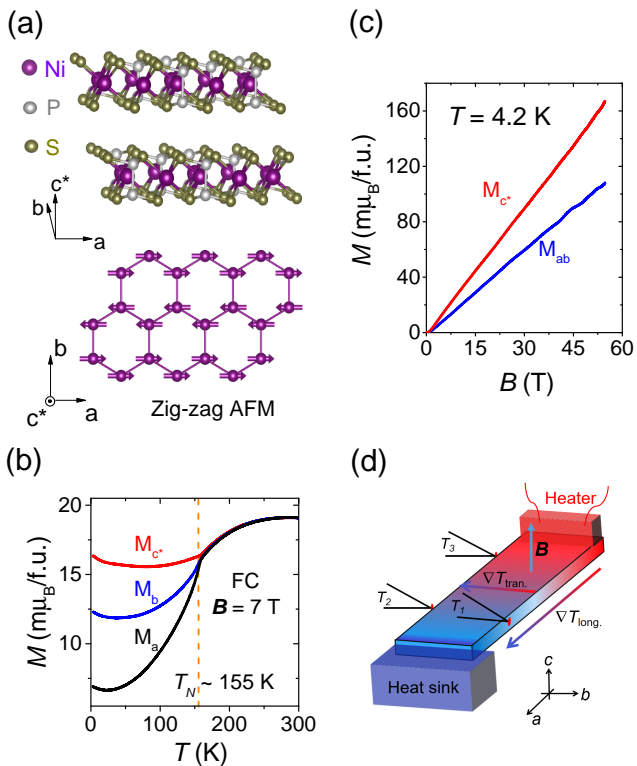


FIG. 1. **Lattice structure, magnetization and thermal transport setup of NiPS<sub>3</sub>.** (a) The lattice structure. The side view (top) shows the layered structure. In each layer, the magnetic nickle atoms (in purple) form the honeycomb lattice, and the magnetic moments are arranged as zigzag chains in ferromagnetically along  $a$  axis but antiferromagnetically along  $b$  axis below the Néel temperature [35, 36], as shown in the top view (bottom). (b) Temperature dependence of magnetization under 7 T with three different orientations. The curves deviate from each other at 155 K, suggesting the antiferromagnetic phase transition, consistent with the previous literature [32]. (c) The high field magnetization up to 55 T at 4.2 K. It doesn't show any transition, indicating a robust antiferromagnetic exchange interaction. (d) The setup for measuring the longitudinal ( $\nabla T_a = -(T_3 - T_2)/l$ ) and transverse ( $\nabla T_b = -(T_2 - T_1)/w$ ) thermal gradients simultaneously.

the exchange energy should exceed 3.2 meV. The largest exchange parameter quantified by inelastic neutron scattering [34, 35] is  $J_3 = 6.9$  meV, which is consistent with our result.

We simultaneously measured the longitudinal and transverse thermal transport responses by using the one-heater-three-thermocouples method, as shown in Figure 1d (see the supplement for more details [41]). Figure 2a displays the temperature dependence of  $\kappa_{aa}$  at 0 T and 14 T. The two curves superpose on top of each other. No strong anomaly is detectable at Néel temperature, confirming that phonons are the almost exclusive carriers of heat.  $\kappa_{aa}(T)$  peaks to 274 W/Km. This is larger than most magnetic insulators, slightly lower than in Cu<sub>3</sub>TeO<sub>6</sub> [14], and well below what is observed for

phonons in non-magnetic insulators like black phosphorus [18] (or diamond, where the peak exceeds 10<sup>4</sup> W/Km [42]), confirming the marginal role of magnons in carrying heat.

Figure 2b shows the field dependence of the thermal Hall conductivity  $\kappa_{ab}$  at three typical temperatures and up to 14 T. The field dependence is always linear, but the amplitude increases drastically from -2.6 mW/Km at 305 K to -910 mW/Km at 33 K. This is much larger than the enhancement of  $\kappa_{aa}$ , implying the thermal Hall angle, the ratio of the two, also increases when cooling.

Figure 2c displays the temperature dependence of  $\kappa_{aa}$  (divided by a factor of -160) and  $\kappa_{ab}$  at 14 T.  $\kappa_{ab}$  does not show any jump at  $T_N$  and peaks, at 25 K and 14 T, to attain a remarkably large peak of -1636 mW/Km.

As observed previously [10, 18],  $\kappa_{aa}(T)$  and  $\kappa_{ab}(T)$  peak at the same temperature. Moreover, the thermal Hall angle, defined as the ratio of  $\kappa_{ab}$  to  $\kappa_{aa}$  divided by the magnetic field, is  $4 \cdot 10^{-4} T^{-1}$ . This remains within a narrow range of  $10^{-4}$ - $10^{-3} T^{-1}$ , where all reported maximal thermal Hall angles lie [18] (see the supplement for more details[41]). The similarity of the Hall angles implies a length scale,  $\lambda_{tha} = \sqrt{\frac{\hbar}{eB} \cdot \kappa_{ab}/\kappa_{aa}}$ , which does not fall below 2 Å in any solid hitherto explored. This is remarkable, since the phonon mean free path at peak temperature in these materials varies from 10 nm to 100 μm. This implies that the thermal Hall angle length is not linked to the mean free path but to one of the two other relevant length scales (the lattice parameter and the phonon wavelength) or a combination of them. In contrast to the phonon mean free path, the interatomic distance and the phonon wavelength at the peak temperature does not vary significantly across these insulating solids.

Proposed theoretical mechanisms of phonon THE [1, 21–31] can be broadly divided into extrinsic and intrinsic. Most extrinsic scenarios invoke specific scattering mechanisms and the phonon mean free path. For example, according to a recent theoretical proposal [28], longitudinal and transverse thermal conductivities can be simply expressed as:  $\kappa_{aa} \sim Cv^2\tau \propto \ell$  and  $\kappa_{ab} \sim Cv^2\tau^2\tau_0^{-1} \propto \ell^2$ . Here,  $C$ ,  $v$ ,  $\tau$ ,  $\ell (= v\tau)$  and  $\tau_0^{-1}$  are respectively the phonon specific heat, the sound speed, the average scattering time, the mean free path and the time-reversal odd skew scattering rate. The two equations imply  $\kappa_{aa} \propto \ell$ ,  $\kappa_{ab} \propto \ell^2$ , and  $\kappa_{ab}/\kappa_{aa} \propto \ell$ , in contrast to experiment, which finds that  $\kappa_{ab}$  and  $\kappa_{ab}/\kappa_{aa}$  have no correlation with  $\ell$ .

Figure 3a and b compare the temperature dependence of  $\kappa_{aa}$  and  $\kappa_{ab}$  in three different samples. As seen in Figure 3a, the longitudinal thermal conductivity  $\kappa_{aa}$  of the three samples fall on top of each other. This is also the case of their specific heat (see the supplement [41]) and, therefore,  $\ell$  is identical in these three samples. On the other hand, the transverse response  $\kappa_{ab}$ , shown in Figure 3b, is very different. In sample #1, it peaks to an amplitude ten times larger than in sample #3, despite

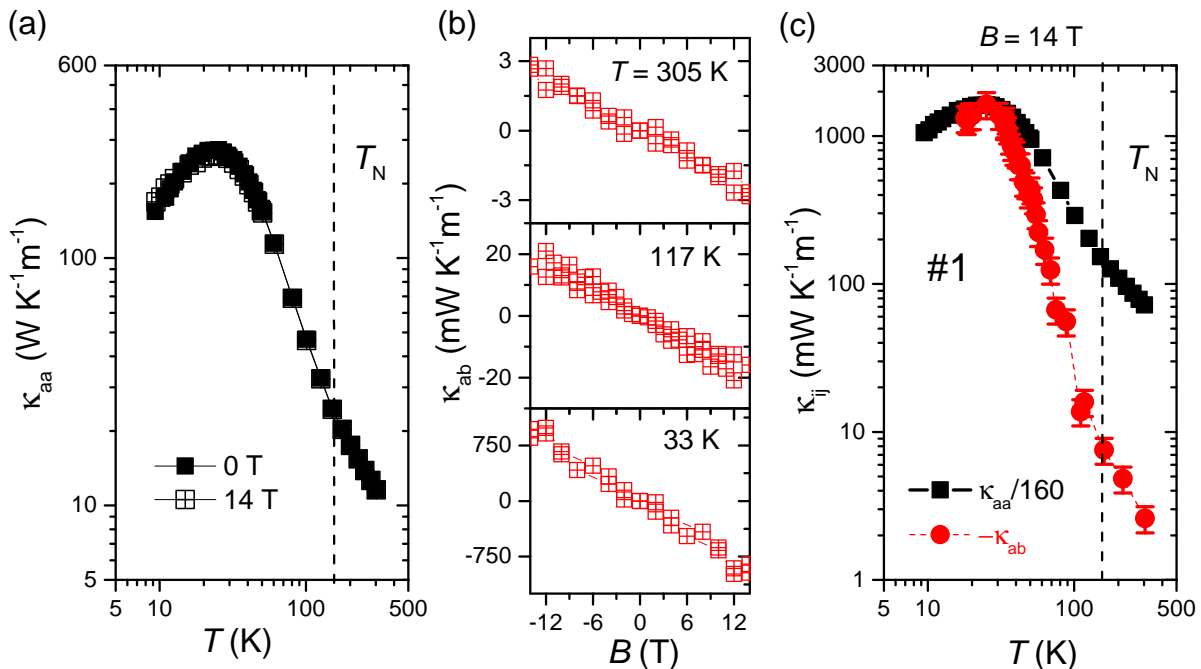


FIG. 2. **Longitudinal and transverse thermal conductivities of NiPS<sub>3</sub>.** (a) Temperature dependence of longitudinal thermal conductivity ( $\kappa_{aa}$ ) under a magnetic field of 0 T and 14 T respectively. Two curves coincide well each other in the whole temperature region with a peak around 25 K. (b) Field dependence of transverse thermal conductivity ( $\kappa_{ab}$ ) at different temperatures with the field sweeping to 14 T. In thermal Hall measurements, the heat current is along  $a$  ( $x$ ) axis, the transverse temperature gradient is along  $b$  ( $y$ ) axis. (c) Comparison of the temperature dependent  $\kappa_{aa}$  (divided by -160) and  $\kappa_{ab}$ .

the fact that their  $\kappa_{aa}$  (and therefore their phonon mean free path) are virtually identical.

An important clue to this variation in the amplitude of  $\kappa_{ab}$  is provided by the magnetization of the three samples. Figure 3c compares the temperature dependence of magnetization  $M$  in three different samples and along three different directions at 7 T.  $M_a$  and  $M_c$  are almost identical, but  $M_b$  has a sample variation. The variation in  $M$  ( $\approx 30\%$ ) is dwarfed by the variation in  $\kappa_{ab}$  ( $\approx 1000\%$ ). Despite this severe mismatch in the amplitude, the variations in magnetization anisotropy and  $\kappa_{ab}$  show a similar trend. Both are the smallest in sample #3 and the largest in sample #1, indicating a role played by the spins. Figure S4 shows the temperature dependence of the in-plane anisotropy of the magnetization in the three samples. In all, magnetization is isotropic in the paramagnetic state, and displays a significant anisotropy below the Néel temperature. As seen in Figure 3d, the variation of transverse thermal conductivity and the magnetization anisotropy ( $M_b - M_a$ ) correlate with each other. Thus, THE is extremely sensitive to a thermodynamic quantity, namely  $M_b$ , the infinitesimal change in the free energy induced by the infinitesimal change in magnetic field along the  $b$ -axis. There is a proportionality between the amplitude of the thermal Hall conductivity and a component of magnetization, which is reminiscent of the celebrated Streda formula [47]. On the other hand, and in sharp contrast, the phonon mean free path is isotropic

in the basal plane (see the supplementary materials [41]) and does not depend on the in-plane anisotropy of the magnetization measured in each sample.

Let us compare NiPS<sub>3</sub> with several other solids displaying THE of variable amplitude. In the case of SrTiO<sub>3</sub>, replacing a tiny fraction of Sr atoms with Ca leads strongly damping of  $\kappa_{xy}$  [16]. This stabilizes a ferroelectric order by hardening of a soft phonon mode, providing evidence for a role played by the soft phonons and an intrinsic scenario involving the hybridization of phonon modes. Such a hybridization has been recently observed by inelastic neutron scattering [48]. However, Ca doping weakens  $\kappa_{xx}$  too (albeit much less than  $\kappa_{xy}$ ) [16], and therefore an extrinsic scenario cannot be ruled out. A second example is provided by the case of Sr<sub>2</sub>IrO<sub>4</sub> [49], in which replacing Ir with Rh first amplifies  $\kappa_{xy}$  before suppressing it when the magnetic order is destroyed. The authors deduce from this observation an extrinsic scenario of scattering by magnetic impurities [31, 49]. However, the evolution of phonon and magnon dispersion with Rh/Ir substitution is not known and one cannot exclude an intrinsic scenario. In contrast with these, no argument in favor of an extrinsic scenario is detectable in our case.

It is also instructive to note similarities and differences between NiPS<sub>3</sub> and  $\alpha$ -RuCl<sub>3</sub>, a solid having attracted tremendous attention in the last few years. Both are van der Waals layers of a honeycomb lattice with a zigzag antiferromagnetic order at zero temperature. However,

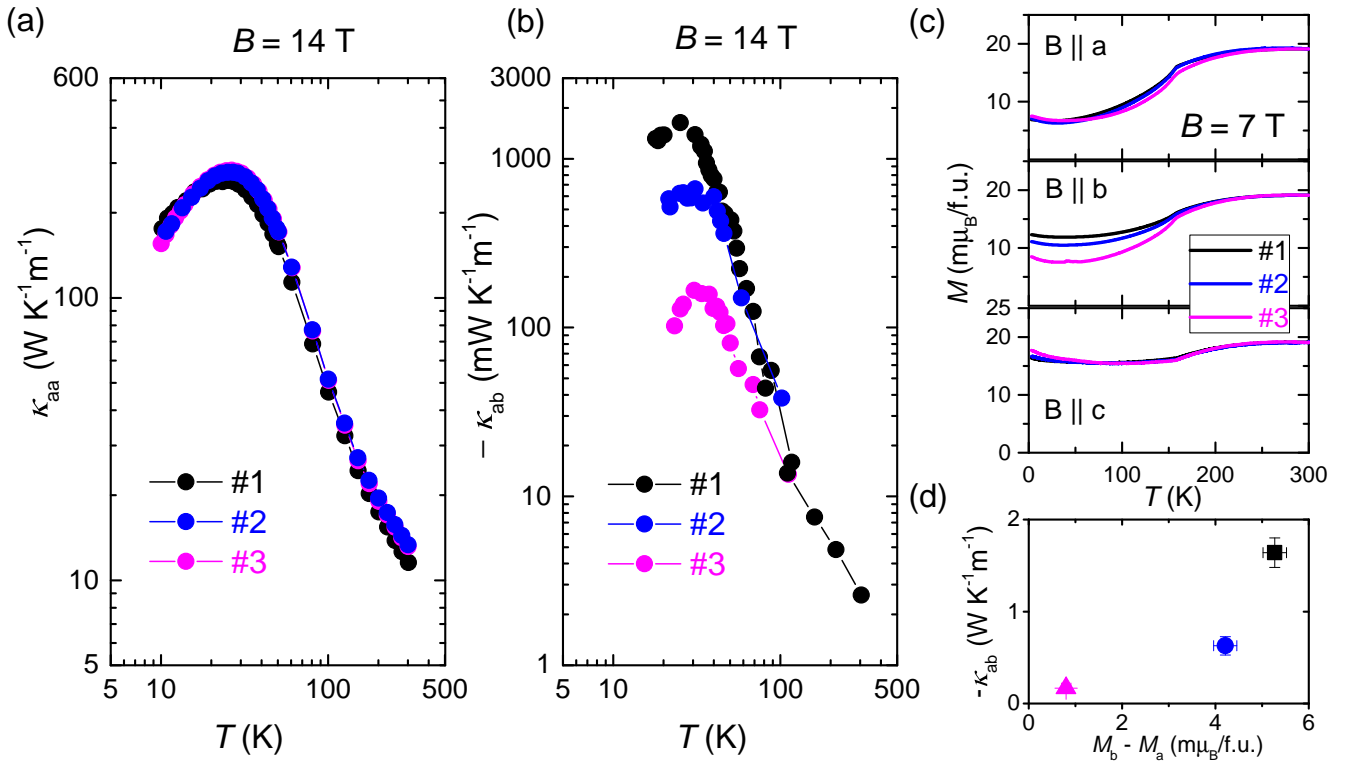


FIG. 3. **Sample dependence of  $\kappa_{aa}$ ,  $\kappa_{ab}$  and magnetization in NiPS<sub>3</sub>.** (a) Comparison of the  $\kappa_{aa}$  in three different samples labeled as #1 (used in Figure 2), #2 and #3. The  $\kappa_{aa}$  overlaps well in different samples, which means that the average scattering rate  $\tau$  and the mean free path  $\ell$  of phonons are consistent in different samples. (b) Comparison of the  $\kappa_{ab}$  in different samples. Contrary to the  $\kappa_{aa}$ , the  $\kappa_{ab}$  is sensitive to samples, having a variation of 10 times among samples. (c) Comparison of the magnetization in different samples and different orientations.  $M_a$  and  $M_c$  have almost no changes,  $M_b$  has a change of about 30%. (d) The peak  $-\kappa_{ab}$  as a function of maximum ( $M_b - M_a$ ) in the three samples.

in the latter, in contrast to the former, one suspects the presence of a sizeable Kitaev term. In this context, it is striking that the longitudinal and the transverse thermal conductivity are both a hundred times larger in NiPS<sub>3</sub> than in  $\alpha$ -RuCl<sub>3</sub> (see the supplemental materials [41]). This observation has profound implications. First, the replacement of well-defined magnons in NiPS<sub>3</sub> by a continuum of incoherent magnetic excitations in  $\alpha$ -RuCl<sub>3</sub> [50] leads to a severe damping of the phonon mean free path. Nevertheless, the thermal Hall angle of the two solids is roughly equal suggesting that what sets this angle neither scales with the phonon mean free path nor varies much by changing the nature of the magnetic excitations coupling with phonons.

Let us now examine what distinguishes three NiPS<sub>3</sub> samples of our study. These crystals are known to be off-stoichiometric due to imperfect occupancy of P and Ni sites [32, 51]. One may suspect, therefore, that the samples differ by the concentration of vacancies. After all, point-like vacancies have little influence of the mean-free-path of long wavelength phonons. But it is unclear why magnetic anisotropy should depend on such vacancies. A more plausible explanation is provided by the presence of twins in crystals of this family. Murayama

and co-workers [52] have shown that there is a rotational twin structure in FePS<sub>3</sub>. Twinned domains share a common  $c^*$ -axis, but are rotated by 120 degrees off each other and are separated by van der Waals stacking faults (See the supplementary materials for more details[41]). Presence of such twins would mix up the genuine responses along the  $a$  and  $b$  axes and damp the in-plane anisotropy of the twinned crystal. This picture would naturally explain the difference between the three crystals studied in this work. Sample #1 which has the highest magnetic anisotropy and the largest thermal Hall effect is the one with lowest level of twinning. Sample #3 is the inverse. As discussed in the supplement [41], we have evidence for twinning in our crystals.

Theoretically, degenerate chiral phonons are known to reside at the center of the Brillouin zone in a honeycomb lattice [53]. The magnetic order in NiPS<sub>3</sub> which breaks inversion center, lifts this degeneracy. Recently, Raman scattering and infrared conductivity have reported on the hybridization between magnons and optical phonons in a sister compound of NiPS<sub>3</sub>, namely FePSe<sub>3</sub> [37, 39, 40]. However, heat is carried by acoustic phonons. Coupling between the latter and magnons has been suggested in other cases [43, 54, 55]. Suppose that magnon and

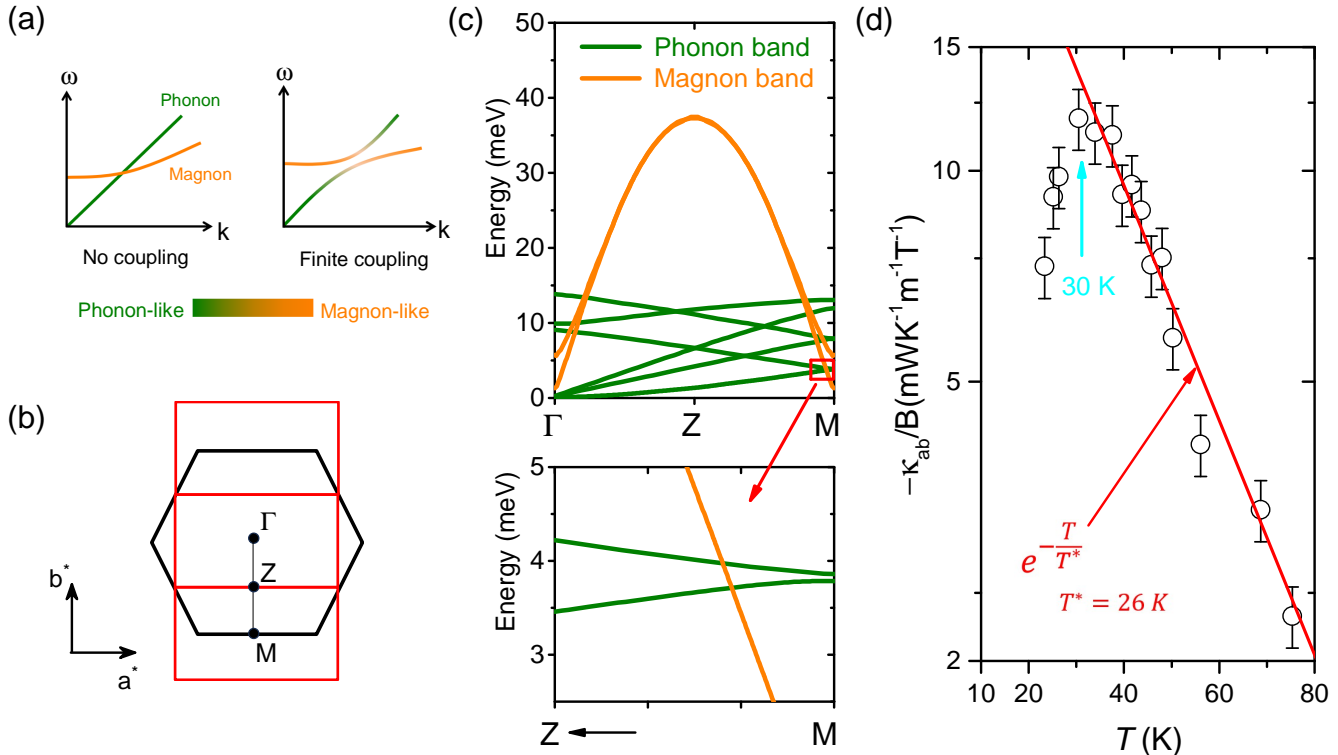


FIG. 4. **Magnon-phonon hybridization and the emergence of a  $\approx 3$  meV energy scale.** (a) Schematic diagram of the magnon-phonon band hybridization (adapted from ref. [43]). (b) Brillouin zone boundaries for magnetic (in red) and crystallographic (in black) Brillouin zones [44]. Note the M-point, which is at the boundary of a crystallographic Brillouin zone and at the center of a magnetic one. (c) The calculated phonon spectrum (in green) [45] and the experimentally derived magnon spectrum [35, 46] of NiPS<sub>3</sub>. Note that the magnon spectrum is identical along  $\Gamma$ -Z and along M-Z. This leads to a magnon-phonon crossing near the M-point. As seen in the lower panel, which is a zoom on the crossing point, this crossing occurs at 3.7 meV. (d) A semi-log plot of  $\kappa_{ab}/B$  as a function of temperature. It peaks at  $\approx 30$  K. Above this temperature, it decreases exponentially compatible with an energy scale of 26 K.

phonon modes cross each other at a point (Figure 4a). In this case, even an infinitesimal coupling will lift the degeneracy, open a gap, and generate two hybrid modes. The lower mode has the capacity to carry heat and generate an odd response to a finite magnetic. We note that in THE material Tb<sub>3</sub>Ga<sub>5</sub>O<sub>12</sub> [2], Petit *et al.*, by performing inelastic neutron scattering, found spectroscopic evidence for mixing between phononic and magnetic modes [56].

Motivated by these considerations, we compared the computed phonon spectrum of NiPS<sub>3</sub> [45] with the magnon spectrum extracted from inelastic neutron scattering measurements [46]. The magnetic ordering generates a new Brillouin zone on top of the nuclear one [35, 46]. The magnetic Brillouin projects rectangles over the hexagons of the honeycomb lattice (See Figure 4b). As a result of this zone folding, a boundary point of the nuclear Brillouin zone is located at the center of a magnetic Brillouin zone. This crucial feature allows magnons to mix up with acoustic phonons. Figure 4c is a representation of band dispersion of magnons and acoustic phonons along  $\Gamma$ -M. One can see that magnon and phonon bands intersect multiply near the  $\Gamma$ - and M- points of the Brillouin zone.

Note that these crossings, in the momentum space, occur along the  $b^*$  and recall that in real space the amplitude of magnetization along the  $b$ -axis was found to set the amplitude of  $\kappa_{ab}$ . Near the M point, the three acoustic phonon branches cross the magnon bands and the lowest crossing occurs at energy of 3.7 meV. A finite coupling at this energy, would open a gap and the lower band of the hybrid mode would saturate to an energy somewhat lower.

Interestingly, our experimental data contains an energy scale of comparable order of magnitude. As previously argued by Yang *et al.* [27], when the thermal Hall effect is intrinsic origin, its temperature dependence in the intermediate regime displays a simple exponential form revealing a characteristic energy, independent of the microscopic details. As seen in Figure 4d, our data reveals such an exponential behavior above the peak at 30 K, with a temperature scale of  $\approx 26$  K. As discussed in the supplementary materials [41], a power law fit to our data is less satisfactory. Such an exponential behavior has been reported in several other cases [8, 9, 19, 27].

Thus, NiPS<sub>3</sub> hosts a large  $\kappa_{ab}$  whose magnitude is ex-

tremely sensitive to the anisotropy of the in-plane magnetization in contrast to the isotropic phonon mean free path. Heat-carrying acoustic phonons cross a magnon branch at an energy somewhat larger than the one extracted from the temperature dependence of  $\kappa_{ab}$ . Taken together, these observations provide a compelling case for an intrinsic THE in this specific case and a promising avenue for investigation of other cases.

Qingkai Meng and Xiaokang Li contributed equally to this work. We thank Benoît Fauqué, Gaël Grissonnanche, Roser Valenti, and particularly Andrew Wildes for helpful discussions. This work was supported by The National Key Research and Development Program of China (Grant No.2022YFA1403500), the National

Science Foundation of China (Grant No. 12004123, 51861135104 and 11574097 ), and the Fundamental Research Funds for the Central Universities (Grant no. 2019kfyXMBZ071). K. B. was supported by the Agence Nationale de la Recherche (ANR-19-CE30-0014-04). X. L. was supported by The National Key Research and Development Program of China (Grant No.2023YFA1609600) and the National Science Foundation of China (Grant No. 12304065).

\* [lixiaokang@hust.edu.cn](mailto:lixiaokang@hust.edu.cn)

\* [zengwei.zhu@hust.edu.cn](mailto:zengwei.zhu@hust.edu.cn)

\* [kamran.behnia@espci.fr](mailto:kamran.behnia@espci.fr)

- 
- [1] N. B. Perkins, Resolving the Achilles' Heel of thermal Hall Conductivity Measurements, *Physics* **15**, 198 (2022).
- [2] C. Strohm, G. L. J. A. Rikken, and P. Wyder, Phenomenological evidence for the phonon Hall effect, *Phys. Rev. Lett.* **95**, 155901 (2005).
- [3] M. Hirschberger, J. W. Krizan, R. J. Cava, and N. P. Ong, Large thermal Hall conductivity of neutral spin excitations in a frustrated quantum magnet, *Science* **348**, 106 (2015).
- [4] T. Ideue, T. Kurumaji, S. Ishiwata, and Y. Tokura, Giant thermal Hall effect in multiferroics, *Nature Materials* **16**, 797 (2017).
- [5] K. Sugii, M. Shimozawa, D. Watanabe, Y. Suzuki, M. Halim, M. Kimata, Y. Matsumoto, S. Nakatsuji, and M. Yamashita, Thermal Hall effect in a phonon-glass  $\text{Ba}_3\text{CuSb}_2\text{O}_9$ , *Phys. Rev. Lett.* **118**, 145902 (2017).
- [6] R. Hentrich, M. Roslova, A. Isaeva, T. Doert, W. Brenig, B. Büchner, and C. Hess, Large thermal Hall effect in  $\alpha\text{-RuCl}_3$ : Evidence for heat transport by Kitaev-Heisenberg paramagnons, *Phys. Rev. B* **99**, 085136 (2019).
- [7] G. Grissonnanche, A. Legros, S. Badoux, E. Lefrançois, V. Zlatko, M. Lizaïre, F. Laliberté, A. Gourgout, J.-S. Zhou, S. Pyon, *et al.*, Giant thermal Hall conductivity in the pseudogap phase of cuprate superconductors, *Nature* **571**, 376 (2019).
- [8] G. Grissonnanche, S. Thériault, A. Gourgout, M.-E. Boulanger, E. Lefrançois, A. Ataei, F. Laliberté, M. Dion, J.-S. Zhou, S. Pyon, *et al.*, Chiral phonons in the pseudogap phase of cuprates, *Nature Physics* **16**, 1108 (2020).
- [9] M.-E. Boulanger, G. Grissonnanche, S. Badoux, A. Alaire, É. Lefrançois, A. Legros, A. Gourgout, M. Dion, C. Wang, X. Chen, *et al.*, Thermal Hall conductivity in the cuprate mott insulators  $\text{Nd}_2\text{CuO}_4$  and  $\text{Sr}_2\text{CuO}_2\text{Cl}_2$ , *Nature Communications* **11**, 1 (2020).
- [10] X. Li, B. Fauqué, Z. Zhu, and K. Behnia, Phonon thermal Hall effect in strontium titanate, *Phys. Rev. Lett.* **124**, 105901 (2020).
- [11] M. Akazawa, M. Shimozawa, S. Kittaka, T. Sakakibara, R. Okuma, Z. Hiroi, H.-Y. Lee, N. Kawashima, J. H. Han, and M. Yamashita, Thermal Hall effects of spins and phonons in kagome antiferromagnet Cd-Kapellasite, *Phys. Rev. X* **10**, 041059 (2020).
- [12] M. Yamashita, J. Gouchi, Y. Uwatoko, N. Kurita, and H. Tanaka, Sample dependence of half-integer quantized thermal hall effect in the kitaev spin-liquid candidate  $\alpha\text{-RuCl}_3$ , *Phys. Rev. B* **102**, 220404 (2020).
- [13] S. Sim, H. Yang, H.-L. Kim, M. J. Coak, M. Itoh, Y. Noda, and J.-G. Park, Sizable suppression of thermal Hall effect upon isotopic substitution in  $\text{SrTiO}_3$ , *Phys. Rev. Lett.* **126**, 015901 (2021).
- [14] L. Chen, M.-E. Boulanger, Z.-C. Wang, F. Tafti, and L. Taillefer, Large phonon thermal Hall conductivity in the antiferromagnetic insulator  $\text{Cu}_3\text{TeO}_6$ , *Proceedings of the National Academy of Sciences* **119**, e2208016119 (2022).
- [15] T. Uehara, T. Ohtsuki, M. Udagawa, S. Nakatsuji, and Y. Machida, Phonon thermal Hall effect in a metallic spin ice, *Nature Communications* **13**, 1 (2022).
- [16] S. Jiang, X. Li, B. Fauqué, and K. Behnia, Phonon drag thermal Hall effect in metallic strontium titanate, *Proceedings of the National Academy of Sciences* **119**, e2201975119 (2022).
- [17] J. Bruin, R. Claus, Y. Matsumoto, N. Kurita, H. Tanaka, and H. Takagi, Robustness of the thermal Hall effect close to half-quantization in  $\alpha\text{-RuCl}_3$ , *Nature Physics* **18**, 401 (2022).
- [18] X. Li, Y. Machida, A. Subedi, Z. Zhu, L. Li, and K. Behnia, The phonon thermal Hall angle in black phosphorus, *Nature Communications* **14**, 1027 (2023).
- [19] M. Gillig, X. Hong, C. Wellm, V. Kataev, W. Yao, Y. Li, B. Büchner, and C. Hess, Phononic-magnetic dichotomy of the thermal Hall effect in the kitaev material  $\text{Na}_2\text{Co}_2\text{TeO}_6$ , *Phys. Rev. Res.* **5**, 043110 (2023).
- [20] R. Sharma, M. Bagchi, Y. Wang, Y. Ando, and T. Lorenz, Phonon thermal Hall effect in charge-compensated topological insulators, *Phys. Rev. B* **109**, 104304 (2024).
- [21] L. Sheng, D. N. Sheng, and C. S. Ting, Theory of the phonon Hall effect in paramagnetic dielectrics, *Phys. Rev. Lett.* **96**, 155901 (2006).
- [22] Y. Kagan and L. A. Maksimov, Anomalous Hall effect for the phonon heat conductivity in paramagnetic dielectrics, *Phys. Rev. Lett.* **100**, 145902 (2008).
- [23] L. Zhang, J. Ren, J.-S. Wang, and B. Li, Topological nature of the phonon Hall effect, *Phys. Rev. Lett.* **105**, 225901 (2010).
- [24] T. Qin, J. Zhou, and J. Shi, Berry curvature and the

- phonon Hall effect, *Phys. Rev. B* **86**, 104305 (2012).
- [25] B. K. Agarwalla, L. Zhang, J.-S. Wang, and B. Li, Phonon Hall effect in ionic crystals in the presence of static magnetic field, *The European Physical Journal B* **81**, 197 (2011).
- [26] J.-Y. Chen, S. A. Kivelson, and X.-Q. Sun, Enhanced thermal Hall effect in nearly ferroelectric insulators, *Phys. Rev. Lett.* **124**, 167601 (2020).
- [27] Y.-f. Yang, G.-M. Zhang, and F.-C. Zhang, Universal behavior of the thermal Hall conductivity, *Phys. Rev. Lett.* **124**, 186602 (2020).
- [28] X.-Q. Sun, J.-Y. Chen, and S. A. Kivelson, Large extrinsic phonon thermal Hall effect from resonant scattering, *Physical Review B* **106**, 144111 (2022).
- [29] B. Flebus and A. H. MacDonald, Charged defects and phonon Hall effects in ionic crystals, *Phys. Rev. B* **105**, L220301 (2022).
- [30] L. Mangeolle, L. Balents, and L. Savary, Phonon thermal Hall conductivity from scattering with collective fluctuations, *Phys. Rev. X* **12**, 041031 (2022).
- [31] H. Guo, D. G. Joshi, and S. Sachdev, Resonant thermal Hall effect of phonons coupled to dynamical defects, *Proceedings of the National Academy of Sciences* **119**, e2215141119 (2022).
- [32] A. R. Wildes, V. Simonet, E. Ressouche, G. J. McIntyre, M. Avdeev, E. Suard, S. A. Kimber, D. Lançon, G. Pepe, B. Moubaraki, *et al.*, Magnetic structure of the quasi-two-dimensional antiferromagnet NiPS<sub>3</sub>, *Physical Review B* **92**, 224408 (2015).
- [33] S. Y. Kim, T. Y. Kim, L. J. Sandilands, S. Sinn, M.-C. Lee, J. Son, S. Lee, K.-Y. Choi, W. Kim, B.-G. Park, *et al.*, Charge-spin correlation in van der waals antiferromagnet NiPS<sub>3</sub>, *Physical Review Letters* **120**, 136402 (2018).
- [34] D. Lançon, R. Ewings, T. Guidi, F. Formisano, and A. Wildes, Magnetic exchange parameters and anisotropy of the quasi-two-dimensional antiferromagnet NiPS<sub>3</sub>, *Physical Review B* **98**, 134414 (2018).
- [35] A. Wildes, J. Stewart, M. Le, R. Ewings, K. Rule, G. Deng, and K. Anand, Magnetic dynamics of NiPS<sub>3</sub>, *Physical Review B* **106**, 174422 (2022).
- [36] S. Kang, K. Kim, B. H. Kim, J. Kim, K. I. Sim, J.-U. Lee, S. Lee, K. Park, S. Yun, T. Kim, *et al.*, Coherent many-body exciton in van der waals antiferromagnet NiPS<sub>3</sub>, *Nature* **583**, 785 (2020).
- [37] S. Liu, A. G. Del Águila, D. Bhowmick, C. K. Gan, T. T. H. Do, M. Prosnikov, D. Sedmidubský, Z. Sofer, P. C. Christianen, P. Sengupta, *et al.*, Direct observation of magnon-phonon strong coupling in two-dimensional antiferromagnet at high magnetic fields, *Physical Review Letters* **127**, 097401 (2021).
- [38] T. Klaproth, S. Aswartham, Y. Shemerliuk, S. Selzer, O. Janson, J. van den Brink, B. Büchner, M. Knupfer, S. Pazek, D. Mikhailova, A. Efimenko, R. Hayn, A. Savoyant, V. Gubanov, and A. Koitzsch, Origin of the magnetic exciton in the van der waals antiferromagnet NiPS<sub>3</sub>, *Phys. Rev. Lett.* **131**, 256504 (2023).
- [39] J. Cui, E. V. Boström, M. Ozerov, F. Wu, Q. Jiang, J.-H. Chu, C. Li, F. Liu, X. Xu, A. Rubio, *et al.*, Chirality selective magnon-phonon hybridization and magnon-induced chiral phonons in a layered zigzag antiferromagnet, *Nature Communications* **14**, 3396 (2023).
- [40] J. Luo, S. Li, Z. Ye, R. Xu, H. Yan, J. Zhang, G. Ye, L. Chen, D. Hu, X. Teng, *et al.*, Evidence for topological magnon-phonon hybridization in a 2D antiferromagnet down to the monolayer limit, *Nano Letters* **23**, 2023 (2023).
- [41] See Supplemental Material for more details (2024).
- [42] D. G. Onn, A. Witek, Y. Z. Qiu, T. R. Anthony, and W. F. Banholzer, Some aspects of the thermal conductivity of isotopically enriched diamond single crystals, *Phys. Rev. Lett.* **68**, 2806 (1992).
- [43] T. Nomura, X.-X. Zhang, S. Zherlitsyn, J. Wosnitzer, Y. Tokura, N. Nagaosa, and S. Seki, Phonon magnetochiral effect, *Phys. Rev. Lett.* **122**, 145901 (2019).
- [44] A. R. Wildes, B. Fåk, U. B. Hansen, M. Enderle, J. R. Stewart, L. Testa, H. M. Rønnow, C. Kim, and J.-G. Park, Spin wave spectra of single crystal CoPS<sub>3</sub>, *Phys. Rev. B* **107**, 054438 (2023).
- [45] A. Hashemi, H.-P. Komsa, M. Puska, and A. V. Krasheninnikov, Vibrational properties of metal phosphorus trichalcogenides from first-principles calculations, *The Journal of Physical Chemistry C* **121**, 27207 (2017).
- [46] A. Scheie, P. Park, J. W. Villanova, G. E. Granroth, C. L. Sarkis, H. Zhang, M. B. Stone, J.-G. Park, S. Okamoto, T. Berlijn, and D. A. Tennant, Spin wave hamiltonian and anomalous scattering in NiPS<sub>3</sub>, *Phys. Rev. B* **108**, 104402 (2023).
- [47] Y. Zhang, Y. Gao, and D. Xiao, Thermodynamics of energy magnetization, *Phys. Rev. B* **102**, 235161 (2020).
- [48] B. Fauqué, P. Bourges, A. Subedi, K. Behnia, B. Baptiste, B. Roessli, T. Fennell, S. Raymond, and P. Steffens, Mesoscopic fluctuating domains in strontium titanate, *Phys. Rev. B* **106**, L140301 (2022).
- [49] A. Ataei, G. Grissonnanche, M.-E. Boulanger, L. Chen, É. Lefrançois, V. Brouet, and L. Taillefer, Phonon chirality from impurity scattering in the antiferromagnetic phase of Sr<sub>2</sub>IrO<sub>4</sub>, *Nature Physics* , 1 (2024).
- [50] S. M. Winter, K. Riedl, P. A. Maksimov, A. L. Chernyshev, A. Honecker, and R. Valentí, Breakdown of magnons in a strongly spin-orbital coupled magnet, *Nature Communications* **8**, 1152 (2017).
- [51] G. Ouvrard, R. Brec, and J. Rouxel, Structural determination of some MPS<sub>3</sub> layered phases (M = Mn, Fe, Co, Ni and Cd), *Materials Research Bulletin* **20**, 1181 (1985).
- [52] C. Murayama, M. Okabe, D. Urushihara, T. Asaka, K. Fukuda, M. Isobe, K. Yamamoto, and Y. Matsushita, Crystallographic features related to a van der waals coupling in the layered chalcogenide FePS<sub>3</sub>, *Journal of Applied Physics* **120** (2016).
- [53] L. Zhang and Q. Niu, Chiral phonons at high-symmetry points in monolayer hexagonal lattices, *Phys. Rev. Lett.* **115**, 115502 (2015).
- [54] I. Živković, Phonons hum a magnetochiral tune, *Physics* **12**, 40 (2019).
- [55] X. Zhang, Y. Zhang, S. Okamoto, and D. Xiao, Thermal Hall effect induced by magnon-phonon interactions, *Phys. Rev. Lett.* **123**, 167202 (2019).
- [56] S. Petit, F. Damay, Q. Berrod, and J. M. Zanotti, Spin and lattice dynamics in the two-singlet system Tb<sub>3</sub>Ga<sub>5</sub>O<sub>12</sub>, *Phys. Rev. Res.* **3**, 013030 (2021).
- [57] Y. Onose, T. Ideue, H. Katsura, Y. Shiomi, N. Nagaosa, and Y. Tokura, Observation of the magnon Hall effect, *Science* **329**, 297 (2010).
- [58] H. Doki, M. Akazawa, H.-Y. Lee, J. H. Han, K. Sugii, M. Shimozawa, N. Kawashima, M. Oda, H. Yoshida,

- and M. Yamashita, Spin thermal Hall conductivity of a kagome antiferromagnet, *Phys. Rev. Lett.* **121**, 097203 (2018).
- [59] A. Kitaev, Anyons in an exactly solved model and beyond, *Annals of Physics* **321**, 2 (2006), january Special Issue.
- [60] K. W. Plumb, J. P. Clancy, L. J. Sandilands, V. V. Shankar, Y. F. Hu, K. S. Burch, H.-Y. Kee, and Y.-J. Kim,  $\alpha$ - $\text{RuCl}_3$ : A spin-orbit assisted mott insulator on a honeycomb lattice, *Phys. Rev. B* **90**, 041112 (2014).
- [61] Y. Kasahara, T. Ohnishi, Y. Mizukami, O. Tanaka, S. Ma, K. Sugii, N. Kurita, H. Tanaka, J. Nasu, Y. Motome, *et al.*, Majorana quantization and half-integer thermal quantum Hall effect in a kitaev spin liquid, *Nature* **559**, 227 (2018).
- [62] E. Lefrançois, G. Grissonnanche, J. Baglo, P. Lampen-Kelley, J.-Q. Yan, C. Balz, D. Mandrus, S. E. Nagler, S. Kim, Y.-J. Kim, N. Doiron-Leyraud, and L. Taillefer, Evidence of a phonon Hall effect in the Kitaev spin liquid candidate  $\alpha$ - $\text{RuCl}_3$ , *Phys. Rev. X* **12**, 021025 (2022).



Supplemental Material for “Thermal Hall effect driven by phonon-magnon hybridization in a honeycomb antiferromagnet” by Q. Meng et al.

### S1. SAMPLES

NiPS<sub>3</sub> single crystals used in this work were synthesized by the chemical vapor transport (CVT) method using I<sub>2</sub> as the transport agent. Polycrystalline NiPS<sub>3</sub> was first synthesized via the solid state reaction of high purity elements of Ni (powder, Alfa, 99.996%), P (lump, Alfa, 99.999%) and S (pieces, Alfa, 99.999%). The mixture were weighed in a stoichiometric ratio and sealed in an evacuated quartz tube and subsequently heated up to 750 °C for 50 hours. Then, the obtained materials were ground, sealed in an evacuated quartz tube with iodine (powder, Alfa, 99.99%) concentration of 3 mg/cm<sup>3</sup>. The tube was transferred into a two-zone furnace with a temperature gradient from 750 °C to 700 °C for one week. The samples show strong diffraction peaks and the hexagonal shape with the size up to millimeters, as shown in Figure S1. They were cut into rectangles (with the long and short side along *a* and *b* axes respectively) and the required dimensions by a wire saw, to fit the thermal transport measurements.

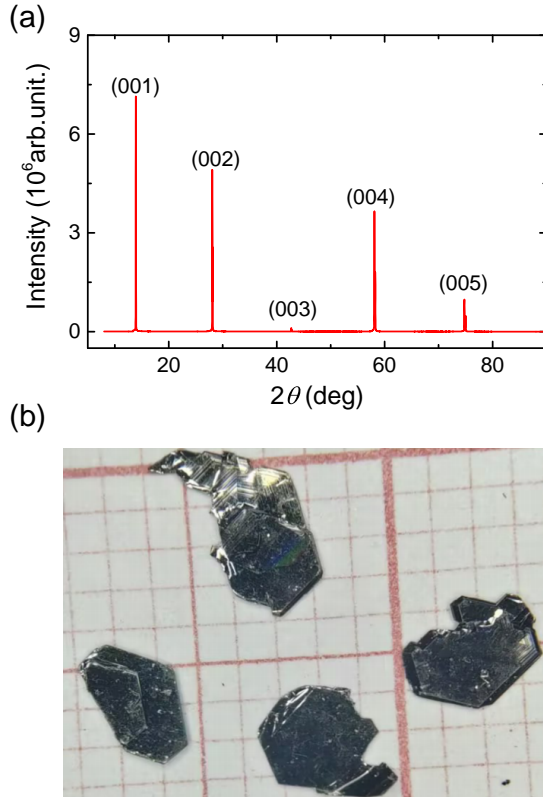


FIG. S1. **X-ray and morphology of the samples** a) X-ray powder diffraction. b) Photograph of NiPS<sub>3</sub> single crystals.

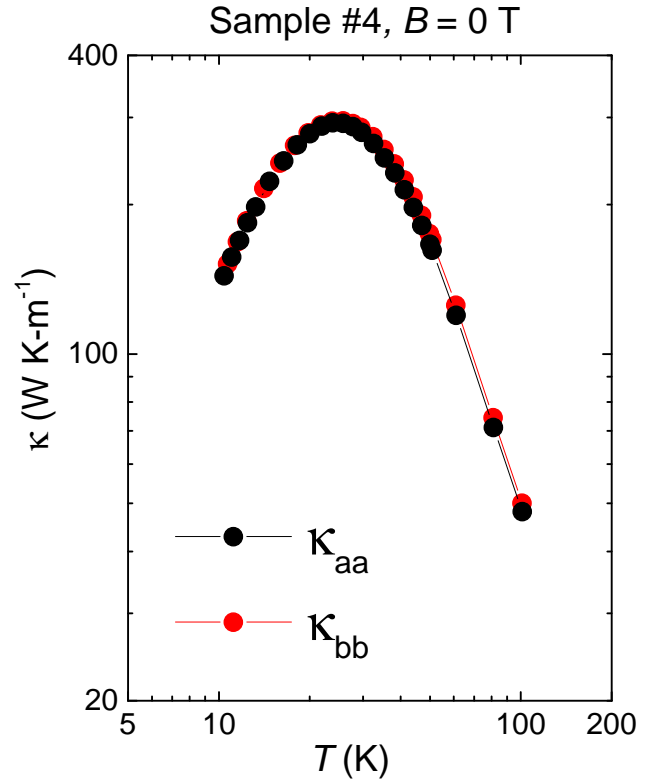


FIG. S2. **Isotropic in-plane longitudinal thermal conductivity.** Temperature dependence of  $\kappa_{aa}$  and  $\kappa_{bb}$  in NiPS<sub>3</sub>.

### S2. MEASUREMENTS

All thermal transport and specific heat experiments were performed in a commercial physical property measurement system (Quantum Design PPMS) within a stable high-vacuum sample chamber. The one-heater-three-thermocouples (type E) method was used for measuring the longitudinal and transverse thermal gradient simultaneously. The thermal gradient in the sample was produced through a 7 kΩ chip resistor alimented by a current source (Keithley6221). The DC voltage on the heater and thermocouples was measured through the DC-nanovoltmeter (Keithley2182A). The thermocouples, the heat-sink, and the heater were connected to samples directly by the silver paste. The longitudinal ( $\nabla T_x = -(T_3 - T_2)/l$ ) and the transverse ( $\nabla T_y = -(T_2 - T_1)/w$ ) thermal gradient generated by a longitudinal thermal current  $J_Q$  were measured. They lead to the longitudinal ( $\kappa_{aa}$ ) and the transverse ( $\kappa_{ab}$ ) thermal conductivity:

$$\kappa_{aa} = \frac{Q}{\nabla T_a} \quad (\text{S1})$$

$$\kappa_{ab} = \frac{\nabla T_b}{\nabla T_a} \cdot \kappa_{aa} \quad (\text{S2})$$

Here  $l$ ,  $w$ ,  $Q$  are the distance between longitudinal thermocouples, the sample width and the heat power respectively, and  $\kappa_{aa} = \kappa_{bb}$  is assumed and verified (see Figure S2).

Magnetization below 7 T were measured in a commercial Superconducting Quantum Interference Device (Quantum Design SQUID). Field-dependent magnetization up to 55 T were measured in a pulsed magnetic field equipment at the Wuhan National High Magnetic Field Center (WHMFC).

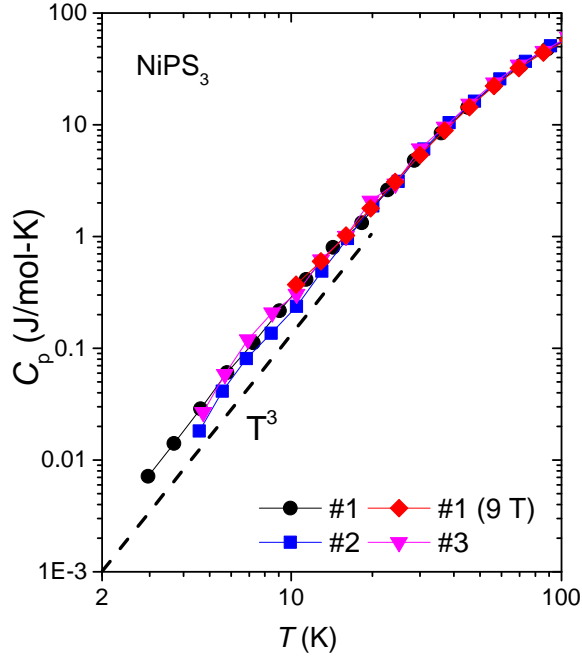


FIG. S3. **specific heat.** Temperature dependence of specific heat in different NiPS<sub>3</sub> samples at zero and finite magnetic field.

### S3. SPECIFIC HEAT

Figure S3 compares specific heat in samples #1, #2 and #3 at zero field and at 9 T. All curves exhibit a coincident behavior, meaning that the mean free path  $\ell = 3\kappa/Cv$  is the same in different samples, and almost unchanged by field.

### S4. IN-PLANE MAGNETIC ANISOTROPY

Figure S4 shows the in-plane magnetic anisotropy ( $M_b/M_a$ ) as a function of temperature. It has the same sample trend with the  $\kappa_{ab}$ , largest in sample #1 and smallest in sample #3.

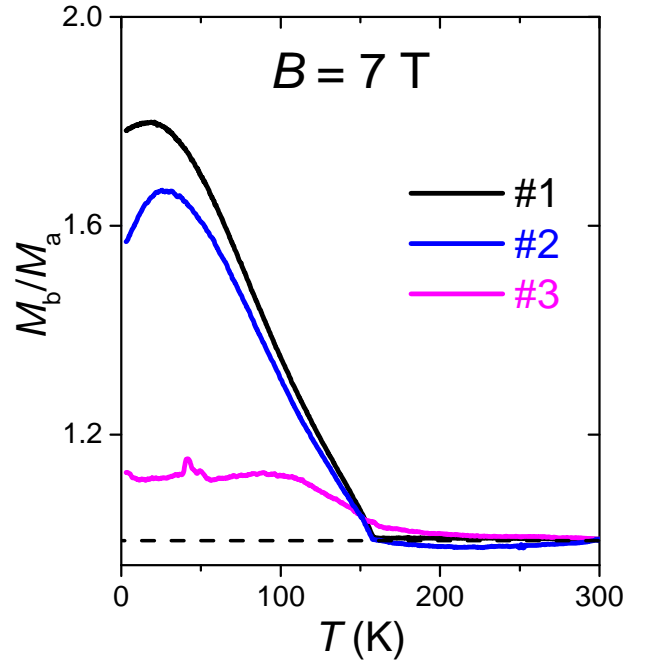


FIG. S4. **In-plane anisotropy of magnetization** The ratio of magnetization along two in-plane axes in three NiPS<sub>3</sub> samples.

### S5. THERMAL HALL ANGLE AND PHONON MEAN FREE PATH

Figure S5 compares longitudinal ( $\kappa_{jj}$ ) and transverse ( $\kappa_{ij}/B$ ) thermal conductivities of different insulators. It can be clearly seen that both the thermal Hall conductivity and the thermal Hall angle of NiPS<sub>3</sub> are close to the record among insulators. Moreover, in different insulators, the longitudinal thermal conductivity  $\kappa_{jj}$  varies by 4 orders of magnitude, but the  $\kappa_{ij}/\kappa_{jj}/B$  ratio remains within the range of  $\approx 10^{-4}$ - $10^{-3}$  T<sup>-1</sup>, indicating the length scale  $\lambda_{tha} = \ell_B \cdot \sqrt{\kappa_{ij}/\kappa_{jj}}$  remains between 2 and 7 Å, comparable to the shortest phonon wavelength allowed by the distance between atoms.

### S6. TWINNED CRYSTAL STRUCTURES

We found that NiPS<sub>3</sub> crystals display a remarkable correlation between the amplitude of the thermal Hall conductivity and the in-plane magnetic anisotropy and attributed the variation and correlation to the presence of twins. In an untwinned crystal (see Figure S6a), in-plane magnetic anisotropy is large. When the stacked structure is twinned (see Figure S6b), the in-plane magnetic anisotropy is attenuated. This would explain the difference between sample #1 and sample #3. When the temperature decreases below  $T_N$ , the  $a$ - and  $b$  lattice parameters decrease and increase respectively (see in Figure S6c)[52]). In a twinned crystal, there would be

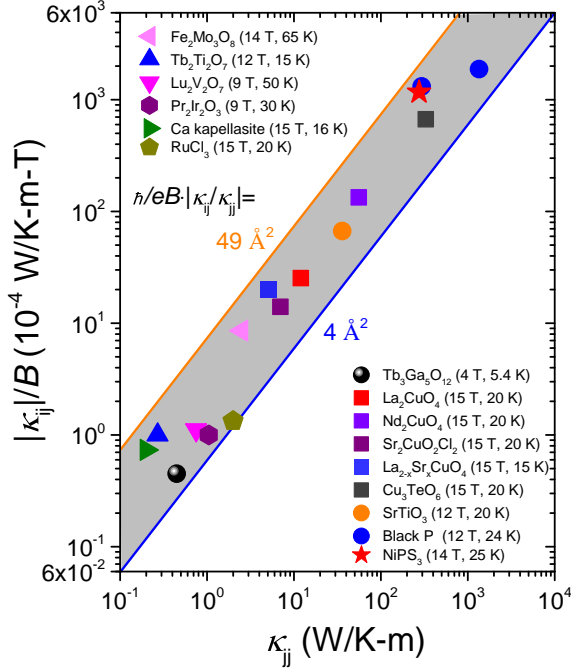


FIG. S5. **Thermal Hall angle in different insulators** The transverse thermal conductivity divided by magnetic field as a function of longitudinal thermal conductivity in different insulators (source: [2, 4, 7–10, 14, 15, 17, 18, 57, 58]).

an alternation of shrinking  $a$ -axis and expanding  $b$ -axis. As a result,  $M_a$  will mix up with  $M_b$  and  $\kappa_{ab}$  will mix up with  $\kappa_{ba}$ . As a result, in a twinned crystal with equal population of three domains, One would find  $\kappa_{ab} = 0$  and  $(M_b - M_a) = 0$ . This explains the correlation seen in Figure 3d.

Figure S7 shows a photograph of a  $\text{NiPS}_3$  sample showing visible twinning along the  $c$ -axis. In Figure S7(a), one clearly sees a stacking feature along the  $c$  direction. In Figure S7(b), the red lines mark three twinned crystals with different stacking orientations, respectively  $c_1$ ,  $c_2$  and  $c_3$ .

## S7. COMPARISON WITH KITAEV CANDIDATES

The Kitaev model [59] describing a honeycomb lattice of spins with bond-dependent interactions has attracted much recent attention because it is an exactly solvable model of a spin liquid. The compound  $\alpha$ - $\text{RuCl}_3$  has emerged as a prominent candidate for Kitaev physics [60]. It has a zigzag antiferromagnetic ground state with a Néel temperature of  $\approx 7$  K, which can be destroyed by a magnetic of  $\approx 10$  T. The observation of a large thermal Hall effect in  $\alpha$ - $\text{RuCl}_3$  [6, 12, 17, 61, 62] has attracted much recent attention. Another Kitaev candidate in which a thermal Hall signal has been detected is  $\text{Na}_2\text{Co}_2\text{TeO}_6$  [19].

Figure S8 compares the longitudinal and the transverse thermal conductivity in  $\text{NiPS}_3$  ( $B = 14$  T), in  $\alpha$ - $\text{RuCl}_3$  ( $B = 15$  T), and in  $\text{Na}_2\text{Co}_2\text{TeO}_6$  ( $B = 16$  T). Both are two orders of magnitude larger in  $\text{NiPS}_3$  compared to the other two. The amplitude of  $\kappa_{xy}$  reported by different groups [6, 12, 17, 61, 62] is not identical. This difference has been attributed to the details of sample growth [12, 17]. However, this sample dependence remains orders of magnitude smaller than the 100-fold variation between  $\text{NiPS}_3$  and  $\alpha$ - $\text{RuCl}_3$ . In other words, while the amplitude of maximum phonon mean free path in different  $\alpha$ - $\text{RuCl}_3$  samples are somewhat different, they remain all  $\approx 100$  times shorter than the phonon mean free path in twinned and untwinned  $\text{NiPS}_3$  crystals. It remains to be seen if this shortening of the phonon mean free path has anything to do with the nature of magnetic excitations in the two systems.

On the other hand, the thermal Hall angle ( $\kappa_{ij}/\kappa_{ii}$ ) in the three solids peaks to the same order of magnitude (Figure S8)(c), implying that the mean free path of phonons does not affect the thermal Hall angle.

## S8. THE EXPONENTIAL TEMPERATURE DEPENDENCE OF $\kappa_{ab}/B$

Figure S9(a)-(b) compares the temperature dependence of  $\kappa_{ab}/B$  in a log-log and a semi-log plot. An exponential (power law) behavior would yield a linear behavior in a semi-log (log-log) plot. The comparison shows that the exponential fit is more consistent with the experimental data.

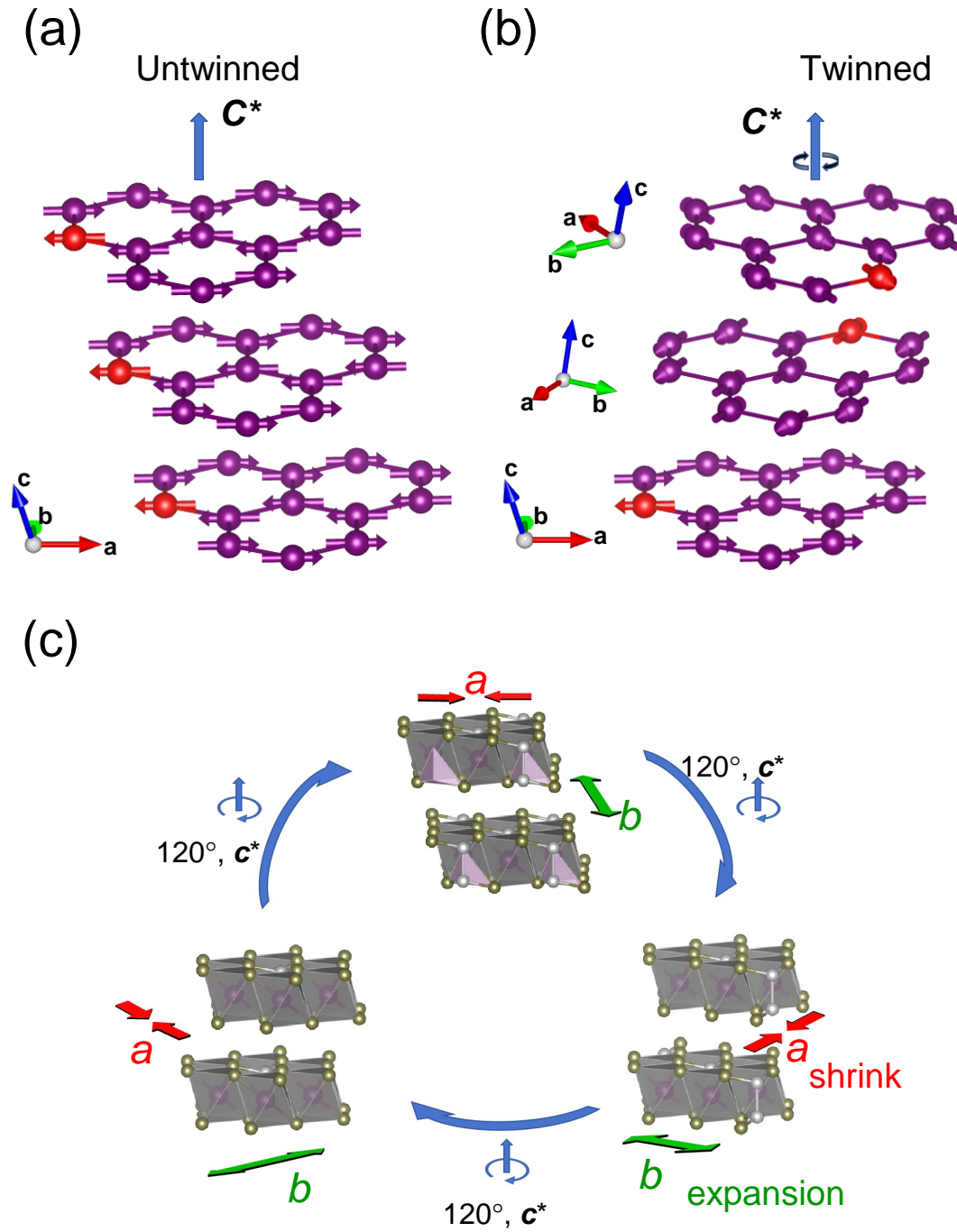


FIG. S6. **Twins.** Schematic diagram of untwinned (a) and twinned (b) NiPS<sub>3</sub> crystal structures. (c) In a twinned crystal, a shrinking  $a$ -axis alternates with an expanding  $b$ -axes across neighboring layers [Taken from the ref. [52]].

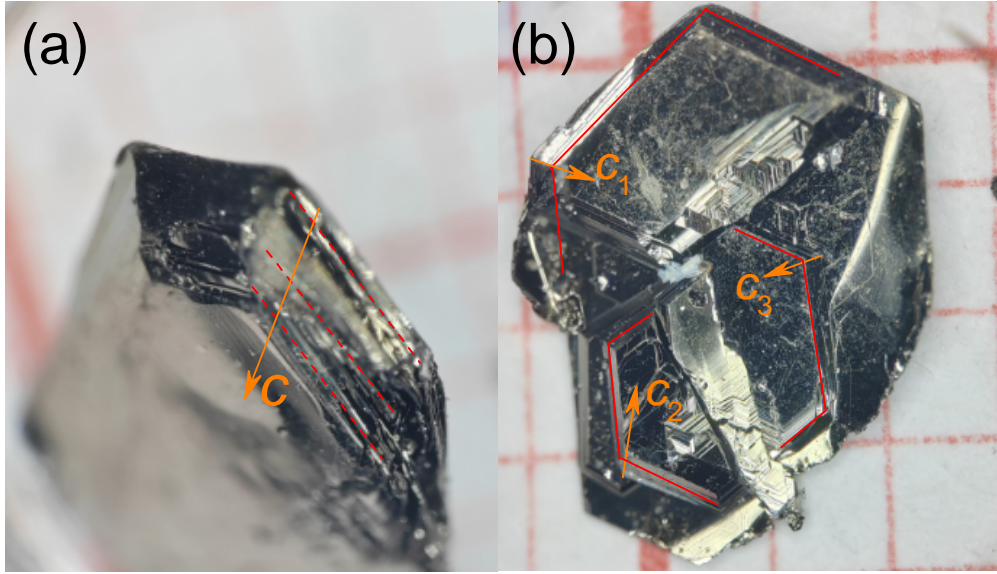


FIG. S7. **Visualising twins in NiPS<sub>3</sub>.** a) The picture of a twinned crystal. b) The same crystal turned over reveals three distinct *c*-axes noted as *c*<sub>1</sub>, *c*<sub>2</sub> and *c*<sub>3</sub>.

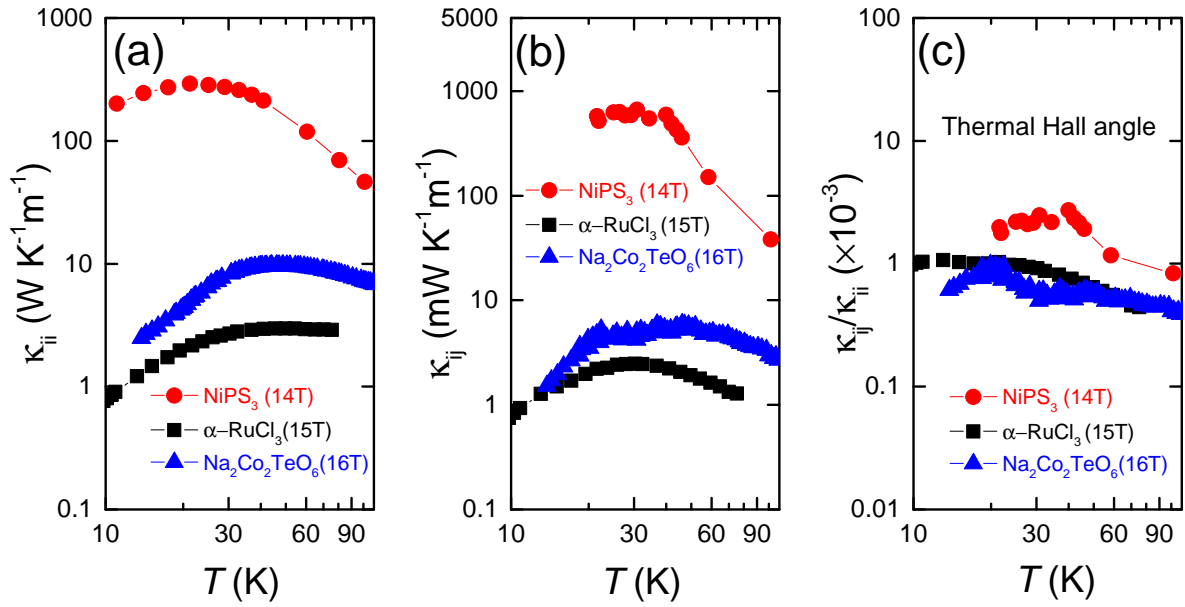


FIG. S8. **Comparison with two Kitaev candidates.** (a)-(b), Longitudinal and transverse thermal conductivity in NiPS<sub>3</sub>,  $\alpha$ -RuCl<sub>3</sub> [62] and Na<sub>2</sub>Co<sub>2</sub>TeO<sub>6</sub> [19]. (c) Temperature dependence of the thermal Hall angle.

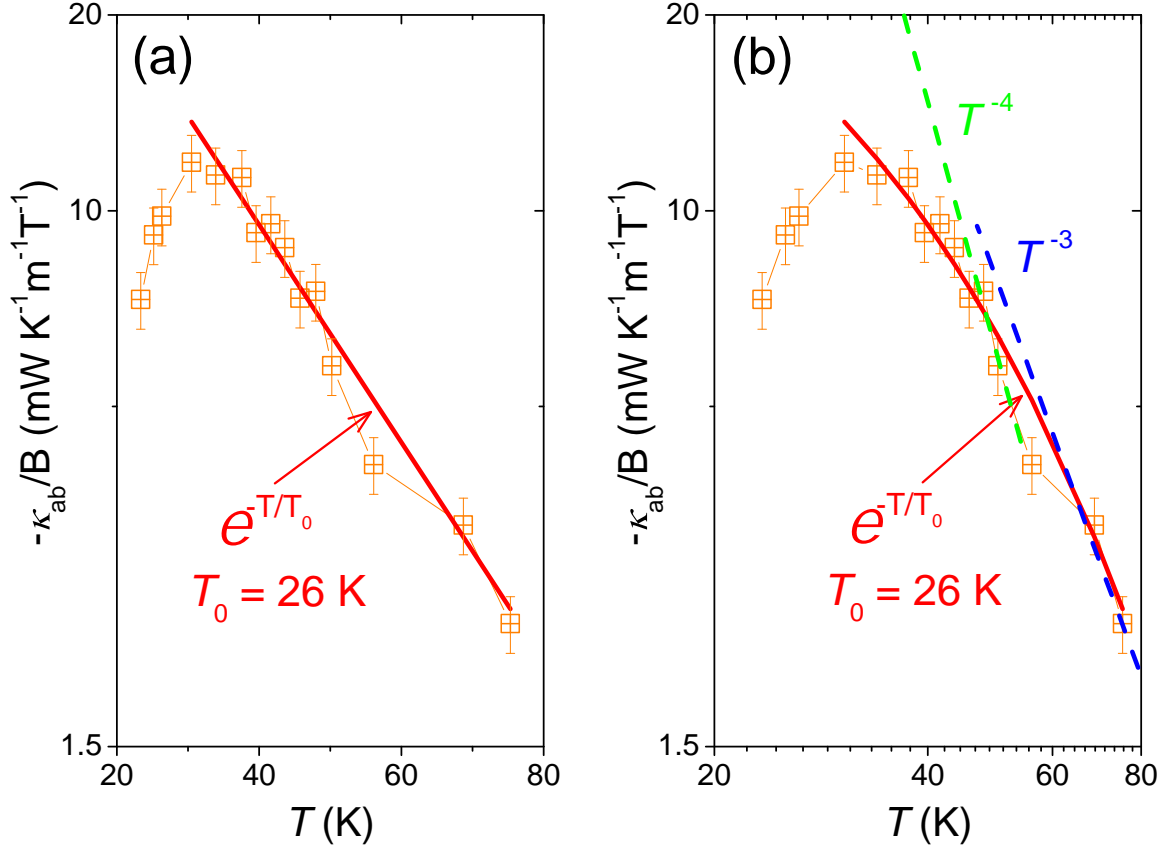


FIG. S9. Comparison of exponential fitting and polynomial fitting result of  $\kappa_{ab}/B$ . Note that the panel a and b were shown in semi-log and log-log plot, respectively.